Multidrug encapsulation within self-assembled 3D structures formed by biodegradable nanoparticles

Claudio Colombo [a], Laura Galletti [a], Maddalena Lepri [a], Ilaria Caron [b], Luca Magagnin [a], Pietro Veglianese [b], Filippo Rossi [a,*], Davide Moscatelli [a]

[a] *Department of Chemistry, Materials and Chemical Engineering "Giulio Natta", Politecnico di Milano, via Mancinelli 7, 20131 Milan, Italy*
[b] *Department of Neuroscience, IRCCS Istituto di Ricerche Farmacologiche Mario Negri, via La Masa 19, 20156 Milan, Italy*

Received 23 January 2015
Received in revised form 26 April 2015
Accepted 28 April 2015
Available online 30 April 2015

1. Introduction

In the last years a lot of efforts and studies were devoted at the design and application of novel drug delivery systems based on nanocarriers [1–4]. This necessity comes from the need to improve classic drug administration routes like oral, intravenous and intraarterial delivery routes [2,5,6]. In particular, the main improvement would be the possibility to maintain drug level in plasma at an effective level for a determined period of time, avoiding under and over dosing [7,8]. Moreover novel drug delivery systems should guarantee: (i) drug protection from hostile environment; (ii) controlled release in response to environment stimuli like pH or temperature; (iii) drug targeting and selectivity to specific organs, tissues or cells thus improving pharmacodynamics characteristic of the drug [9,10]. In this framework, a great deal of effort is now focusing on the engineering of nanoparticulate systems, which has led to the development of various types of drug-loaded nanocarriers, such as liposomes, nanoparticles (NPs) and micelles able to serve as efficient diagnostic and/or therapeutic tools against severe diseases, such as cancer, infectious or neurodegenerative disorders [11–14]. These carriers can present

* Corresponding author.
E-mail address: filippo.rossi@polimi.it (F. Rossi).

different sizes and can be functionalized with different molecules to meet several therapeutic needs [15,16]. Furthermore they can work as vehicle for targeted therapies due to their capacity to cross biological barriers, entering and releasing their payload within cells [3,17]. Thus, NPs specific characteristics make them promising materials in many fields. However, they present some drawbacks. Indeed, direct injection of colloidal NPs suspension to the target tissue could lead to uncontrolled diffusion over the zone of injection, as they are not confined by any support. In addition, NPs could easily extravasate into the bloodstream, migrating all over the body, especially to the liver and the spleen, resulting in unwanted and dangerous accumulation [18,19]. According to these critical issues, the possibility to build macrostructures starting from NPs through self-assembly can be a way to overcome these problems [20–22].

Indeed, NPs can be assembled into macrostructures which can reach final dimensions greater than the nanometric scale, without losing the typical properties of nanoscale structures; e.g., NPs assemblies retain the optical, magnetic, electrical, biological, and mechanical properties, typical of NPs [23]. Moreover, these assemblies are non-chaotic, but organized according to a predetermined pattern and involve large numbers of NPs [4]. The assembly process can be originated by a variety of interparticle interactions, mainly van der Waals forces, dipole–dipole, London, hydrogen bonding, electrostatic forces and entropic effects, or other interactions. Alternatively, it can be driven by external fields, such as electrical, magnetic or gravitational [24,25].

In this work, we describe a novel self-assembled 3D structure formed by biodegradable NPs able to swell in physiological conditions and that can be used for multiple release of hydrophilic and hydrophobic drugs. To the best of our knowledge these multiple drug delivery systems are generally constituted by different loaded polymers layered one above the other [26,27]. With the approach here presented hydrophobic drugs could be loaded within NPs, while hydrophilic ones remain trapped in the aqueous interstices that they create during NPs assembly. The key point is to maintain the advantages typical of polymeric NPs as drug delivery reservoir and degradability, together with the advantages of macrostructures, like easy handling and swelling ability. In this perspective, we used NPs with different superficial charges and we took advantage of their electrostatic interaction to build a 3D macrostructure. In particular, we synthesized NPs through a surfactant-free two-step process. In the first step we synthesized a macromonomer from 2-hydroxy-ethyl methacrylate (HEMA) grafted with poly-ε-caprolactone (PCL) chains controllable in terms of both length and composition as reported in literature [28,29]. In the second step we conducted an emulsion free radical co-polymerization of the macromonomer together with methacrylic acid (MAA) and either [2-(Methacryloyloxy)ethyl] trimethyl ammonium chloride (HEMA-Ch^+) or 3-sulfopropyl methacrylate potassium salt (HEMA-SO_3^-). In this work we used MAA to help, via hydrogen bonding, to entrap hydrophilic molecules through water swelling while HEMA-Ch^+ and HEMA-SO_3^- provide positive and negative superficial charges to the NPs respectively.

The macrostructure assembled by the mixing of positive and negative NPs at room temperature was then characterized and the possibility to provide multiple drug delivery was then studied using two commonly used drug mimetics: a hydrophilic one (sodium fluorescein [30]) and a hydrophobic one (To-Pro3 [17]) proving the possibility to encapsulate and deliver different drugs in a different and tailored way.

2. Experimental section

2.1. Materials

For the macromonomer synthesis ε-caprolactone (CL, 99%), 2-hydroxyethyl methacrylate (HEMA, ⩾99%) and 2-ethylhexanoic acid tin(II) salt ($Sn(Oct)_2$, ∼95%) were all purchased from Sigma–Aldrich (Germany) and used without further treatment. For NP synthesis methacrylic acid (MAA), 3-sulfopropyl methacrylate potassium salt (HEMA-SO_3^-), [2-(Methacryloyloxy) ethyl] trimethyl ammonium chloride (HEMA-Ch^+), potassium persulfate (KPS; ⩾99%) and 2,2′-Azobis(2-methylpropionamidine) dihydrochloride (AAPH) were purchased from Sigma–Aldrich (Germany) and used without further treatment. For *in vitro* drug delivery studies sodium fluorescein (SF) was purchased by Sigma–Aldrich (Germany) and To-Pro3 (To-Pro) by Invitrogen (Italy).

2.2. Synthesis and characterization of HEMA-CL macromonomers

Macromonomers used for NPs synthesis were obtained through a ring opening polymerization reaction (ROP) using a procedure reported in literature [31]. Briefly, reaction was carried out in bulk conditions, without using any solvent. 10 g of CL were heated up in a stirred flask at 130 ± 1 °C with the temperature controlled by an external oil bath. A mixture of $Sn(Oct)_2$ and HEMA at a given molar ratio (1/400) was prepared and left under continuous magnetic stirring at room temperature until the complete dissolution of $Sn(Oct)_2$.

Then, HEMA solution composed of 3.8 g of HEMA and 29 mg of $Sn(Oct)_2$ was then added to CL (with a CL/HEMA molar ratio equal to 3) to initiate the reaction, which was carried out for two hours. The reaction product consists to a HEMA molecule functionalized with 3 units of CL (herein after reported as HEMA-CL_3). It was refrigerated at 4 °C waiting for further use. Macromonomer molecular weight (MW) and thus the average chain length n (the average number of CL unit added to HEMA molecule, theoretically equal to 3 in this work) characterization was carried via ^1H NMR was performed using a 400 MHz Ultrashield NMR spectrometer (Bruker, Switzerland) by dissolving the sample in $CDCl_3$.

2.3. Synthesis of positive and negative NPs

The macromonomer synthesized in the previous section was used in emulsion polymerization processes in order to produce final NPs [28,29].

2.3.1. Positively charged NPs

Polymerization was carried out in a 50 mL three necked glass flask in batch condition: 0.075 mL of HEMA-Ch^+, 0.125 mL of MAA and 2.3 g of HEMA-CL_3 were added to 50 mL of distilled water and the solution was heated up to 80 °C and kept under an inert atmosphere obtained after vacuum–nitrogen cycles. The reaction was initiated by the injection of 0.04 g of AAPH used as initiator. Reaction was run for three hours, then the obtained latex was filtered and conserved at 4 °C until use.

2.3.2. Negatively charged NPs

Polymerization was carried out in a 50 mL three necked glass flask in semi-batch condition: 0.075 g of HEMA-SO_3^- and 0.125 mL of MAA were added to 50 mL of distilled water, the solution was heated up to 80 °C while an inert atmosphere was obtained after vacuum-nitrogen cycles. The macromonomer HEMA-CL_3 (2.3 g) was injected with a rate of 2 mL/h using a syringe pump (Model NE-300, New Era Pump System, US). KPS (40 mg) was used as the initiator and added at the begin-ning of the macromonomer injection. Reaction was run for three hours, then the obtained latex was filtered and conserved at 4 °C until use.

The percentage of MAA used for positive and negative NPs was optimized in order to guarantee swelling ability on one side, but not compromise degradability of NPs on the other. Also, higher content of MAA lead to difficulties in the obtainment of monodispersed nanoparticles due to its hydrophilicity.

2.4. NP characterization: DLS and TEM analyses

Final particle size was determined by DLS (Malvern, Zetanano ZS, US); analyses were performed in triplicate and reported data show the average of three runs where the standard deviation was always below 5%. Size and morphology of produced NPs were also confirmed by transmission electron microscopy (TEM; using an EFTEM Leo 912AB, at 80 kV, by Karl Zeiss, Jena, Germany).

Samples were prepared placing 5 μL drop of NP dispersion on a Formvar/carbon-coated copper grid and dried overnight. Digital images were acquired by a charge-coupled device (CCD; Esi Vision Proscan camera).

2.5. Atomic force microscopy (AFM)

AFM analysis was carried out for the characterization of both NP latexes using an NT-MDT Solver Pro instrument operating in non-contact mode with silicon tips. Samples were prepared by dropping latexes onto silicon substrate and drying. AFM images on 1 × 1 μm areas were recorded for the preliminary morphologic evaluation; 500 × 500 nm image were then cropped and height line profile performed for single NP. Surface morphology was evaluated by flattening the images (first order) using NT-MDT software.

2.6. Self-assembled 3D structure preparation and yield

Positively charged NPs were inserted in a 10 mL vial and the negative ones were slowly dripped into it (1:1 volume ratio). The solid content for both latexes was adjusted to 2.5% w/w with distilled water before this procedure. The aggregation process is visible through the formation of a white solid-like material and it is evident a transition of the liquid from a white tone to a transparent one.

Aggregation yield reveals how much solid structure is formed starting from a certain amount of NPs dispersion.
It was calculated as the ratio between the mass of the solid after lyophilization and the effective mass of the initial NPs, both the positive and negative ones, as reported in Eq. (1):

$$\text{yield} = \frac{m_{\text{solid}}}{m_{\text{NPs}^+} + m_{\text{NPs}^-}} \cdot 100 \tag{1}$$

where m_{solid} is the mass of the solid formed (measured after lyophilization), $m_{\text{NPs+}}$ is the actual mass of the positive NPs used for aggregation and $m_{\text{NPs}-}$ the mass of negative NPs. Both these parameters were evaluated through thermogravimetric measure of the produced NP latexes.

2.7. Scanning electron microscopy (SEM)

Environmental scanning electron microscopy analysis of the produced solids was performed on gold sputtered samples at 10 kV with Evo 50 EP Instrumentation (Zeiss, Jena, Germany). To preserve the actual morphology of the 3D structure under complete swelling, freeze-drying (24 h) was applied to remove all the liquid phase by sublimation.

Because of the low operating values of temperature and pressure, the polymer chains were expected to retain the same conformation they had in wet conditions.

2.8. Swelling behavior

To assess swelling kinetics, solid samples were freeze-dried, weighted (W_d) and poured in excess of PBS to achieve complete swelling at 37 °C in 5% CO_2 atmosphere. The swelling kinetics was measured gravimetrically: samples were removed from PBS at regular time points, they were wiped with moistened filter paper in order to remove the excess of PBS and then weighed (W_t). Swelling ratio is defined as follows:

$$\text{swelling ratio} = \frac{W_t - W_d}{W_d} \cdot 100 \tag{2}$$

where W_t is the weight of the wet material as a function of time and W_d of the dry one.

2.9. To-Pro and SF loading and delivery

As said To-Pro and SF were chosen mainly because of their steric hindrance, similar to many small drugs, and for their absorbance that makes them easily detectable by UV spectroscopy. Moreover, they mimic the behavior of hydrophobic (To-Pro) and hydrophilic (SF) agents that could be delivered by the 3D macrostructure. To-Pro was loaded into NPs after the polymerization reaction. Firstly, the concentration of the positively-charged NPs was increased under vacuum at room temperature with the use of a Rotavapor apparatus (Buchi instruments). 1 ml of NP latex (25% w/w) was obtained with the absence of aggregates as confirmed by DLS measurements. The concentrated latex was incubated with 20 μg To-Pro for one day at room temperature under gentle magnetic stirring. Latex was then diluted to the desired concentration (i.e. 2.5% w/w). Loading efficiency was evaluated by precipitating the NPs and evaluating the drug in the supernatant according to the literature [17], using Eq. (3):

$$\%\ \text{loading} = \frac{\text{drug entrapped in NPs}}{\text{initial amount of drug added}} \tag{3}$$

SF (0.1 mg/mL) was loaded before aggregation through its addition to the negatively charged latex and then dropped into the positive one. The solid content for both latexes was 2.5% w/w.

At the end of this process, SF molecules remain solvated into water which is entrapped in the pores of the 3D macrostructures. Self-assembled structures, loaded with To-Pro and SF, were placed in excess of phosphate buffered saline solution (PBS) at 37 °C and aliquots were collected at defined time points, while the sample volume was replaced by fresh PBS, in order to avoid mass-transfer equilibrium with the surrounding solution. Percentage released of To-Pro and SF was measured by spectroscopy from the supernatant. Results were expressed as average percentage released ± standard deviation, $n = 3$.

2.10. Cell culture

Mouse fibroblasts (L929) were cultured in complete medium (Dulbecco' s modified Eagle's medium (DMEM) supplemented with 10% fetal bovine serum, 1% penicillin/streptomycin, 1% L-glutamine 200 mM). Cells were maintained at 37 °C in 5% CO_2 and used.

2.11. Cytocompatibility

3D macrostructures were formed and located into cell culture inserts (Falcon, 1.0 μm pore size). L929 were seeded in 24-well plates at concentration of 50,000 cells/well in 1 mL complete medium and grown at 37 °C, 5% CO_2. After 24 h, the medium was changed and the inserts with 0.2 mL of self-assembled NPs were added in contact with the medium.

After 3 days of culturing, the cytotoxicity of macrostructure was evaluated by performing an MTS assay [17,32]. The absorbance was measured at 570 nm, and the results were compared with that of the control wells to determine relative cell viability.

2.12. Statistical analysis

Where applicable, experimental data were analyzed using Analysis of Variance (ANOVA). Statistical significance was set to p value < 0.05. Results are presented as mean value ± standard deviation.

3. Results and discussion

Polymer NPs were obtained through a solvent free synthesis composed of two steps, summarized in Fig. 1A. Ring opening polymerization (ROP) allows to obtain short and controllable PCL-based macromonomers and confers the biodegradability of

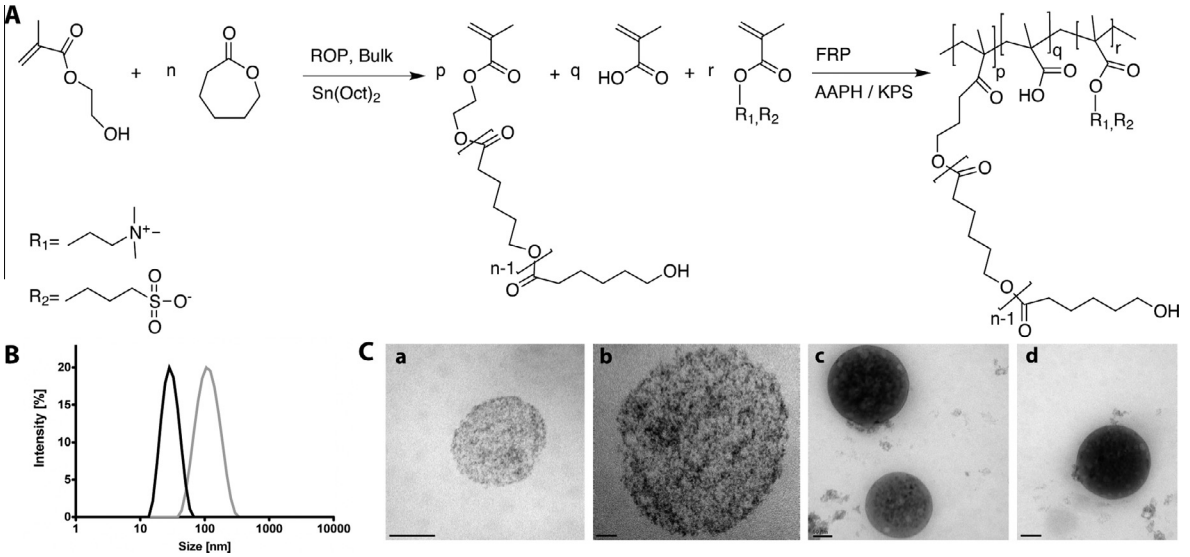

Fig. 1. (A) Synthetic route of positive (HEMA-CL-MAA-Ch) and negative (HEMA-CL-MAA-SO_3^-) NPs; (B) DLS measurement of NPs (grey: positive NPs; black: negative NPs,); (C) TEM pictures of positive NPs (a and b) and negative ones (c and d) (scale bars: (a) 100 nm, (b) 30 nm, (c and d) 20 nm).

the NPs [28,29]. The study of the influence of the PCL chain length on the final NPs characteristics has already been investigated [29]. In general the role of the CL chain length is the modulation of the NPs dimension: for comparable synthesis condition a longer CL chain leads to smaller NPs due to the increase in hydrophobicity of the starting macromonomer. In this work we decided to use CL_3 because NPs produced from this macromonomer have been studied and investigated both in *in vitro* and *in vivo* context [3] concerning their biodegradability, cellular uptake and degradation. The second step involves the emulsion free radical polymerization (FRP) of the produced macromonomers. In this step HEMA-CL_3 macromonomer was copolymerized via FRP with MAA and different stabilizing agents: HEMA-Ch^+ for positively charged NPs and HEMA-SO_3 for negative ones. The resulting NPs present narrow size distribution as visible from DLS and TEM analyses presented in Fig. 1B and C. Final diameter was smaller for negative NPs and ζ-potential values presented in Table 1 evidence the opposite charged nature of the NPs synthesized.

The surface morphology of both NPs was analyzed also with AFM and the respective images are given in Fig. 2. The results indicated that the surface of positive and negative NPs were nearly spherical in shape with a smooth surface. In accordance with DLS and TEM analyses NPs were found to have different characteristic dimension: positive in the range of 130 nm and negative in the range of 65 nm. These results are completely consistent with DLS and TEM considering the differences of the techniques.

Self-assembly of NPs was obtained dropping equal volume of choline-based NPs (positive) into 3-sulfopropyl methacrylate-based ones (negative). After aggregation, a white semisolid was obtained (Scheme 1) with a totally transparent supernatant, underlining the absence of NPs in the liquid solution, as confirmed by DLS analysis (data not shown). The aggregation yield revealed that 85% of the polymer latex volume was converted in 3D macrostructure. This process is high reproducible and consents to form a single aggregate able to release hydrophilic and hydrophobic drugs.

To obtain insight into the three-dimensional (3D) structure of the network formed we used SEM analysis. Samples were prepared by a freeze-drying method followed by coating a thin layer of gold prior to SEM imaging. There are some previous works on SEM morphology of dried biopolymers and scaffolds in general, but much care must be taken when making the dried samples for SEM analysis, since the removal of water held within the porous structure may disrupt the structural stability and result in collapse and some artifacts upon drying [33]. Our results, reported in Fig. 3, revealed that dried self-assembled material possesses a highly entangled structure (Fig. 3A–C). More details were observed in the SEM image with higher amplification (Fig. 3D–F). Indeed the cross-sectional interior structure exhibited high porous structure. The pores assumed an irregular shape but they were well distributed all along the structure.

Table 1
Characteristics of the synthesized NPs measured with DLS.

	Post synthesis			Post drug loading	
	Diameter (nm)	PDI	ζ-potential (mV)	Diameter (nm)	PDI
Positive NPs	134.8	0.034	30	153.7	0.045
Negative NPs	48.5	0.057	−25		

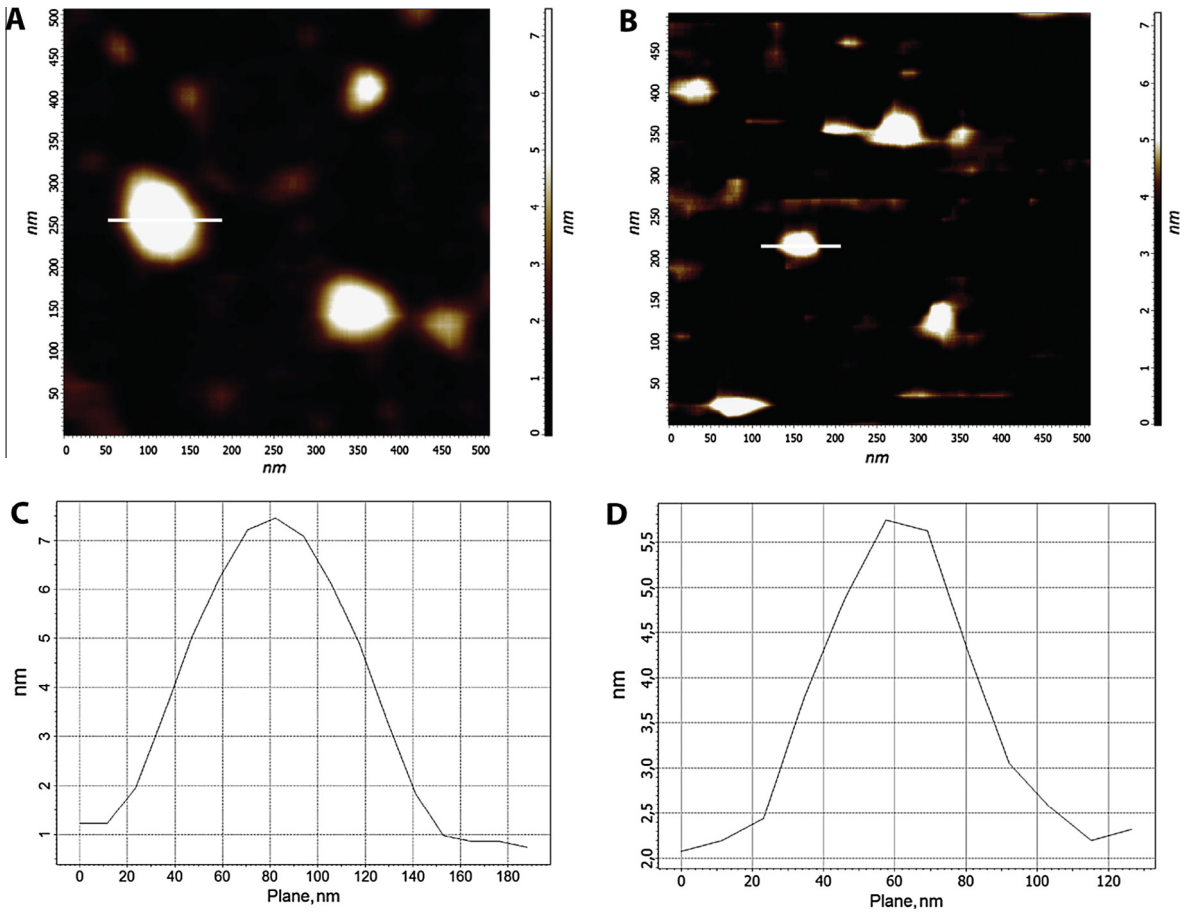

Fig. 2. AFM images of NPs prepared from HEMA-CL macromonomer with different superficial charges: (A) positive NPs, (B) negative NPs. The corresponding size profiles are visible in (C) and (D).

The thickness of the wall was approximately less than 10 μm and it demonstrates that these macrostructures present the microscopic porous structure with a complex 3D construction in the dried state. Although not all the pores were precisely the same size, they were distributed over these different size ranges. The interconnection of the pores seemed to be well homogeneous along the network and confirms the suitability of these aggregates as macrostructure for biomedical purposes [34,35].

Swelling ratio has been widely used as a simple method to characterize water absorption and stability of biomaterials. Here the ability to retain aqueous solutions of the 3D macrostructure as swelling kinetics in water and PBS was examined at 37 °C and the results are presented in Fig. 4. The swelling profiles can be divided into two regions (A and B), i.e., the first one, which took place in the first 6 h (up to a quasi-equilibrium), and the second one that ended after 24 h (to an equilibrium condition), then the system reached the swelling equilibrium that allows the loading of hydrophilic molecules within the macrostructure. At the beginning, starting from dry network, water started to fill up the micro pores which can be easily accessed, as visible from SEM analysis (Fig. 3). After 8 h the swelling ratio of the 3D macrostructure reached 41.07 ± 3.49 in water and 29.21 ± 3.26 in PBS. Then we can easily observe the presence a second pattern of swelling until 64.17 ± 3.46 in water and 48.15 ± 2.84 in PBS. This could be attributed to two different mechanisms: at the beginning water enters within the network until the first equilibrium (A), then water can enter swelling NPs and increasing so the amount of water retained (B) reaching the complete swelling equilibrium. In addition, the different behavior in water and in PBS could be observed in Fig. 4. The swelling ratio in PBS is smaller than in water and this could be explained considering that PBS presents much higher ionic strength (0.16 M) than the water (close to 0 M), therefore the 3D structure loses water due to the osmotic pressure. This effect surpasses the water absorption ability of the 3D macrostructure which leads the sample weight decreasing [36].

To test our hypothesis that self-assembled NPs can work as reservoir sustaining the multiple release of hydrophilic and hydrophobic drugs, the release of SF and To-Pro was examined after incubation at 37 °C. The aim of this system is to deliver drugs and then degrade with consequent drug release driven only by concentration gradient. Here PCL chain length was optimized in order to not interfere with drug delivery kinetics, allowing pure Fickian diffusion.

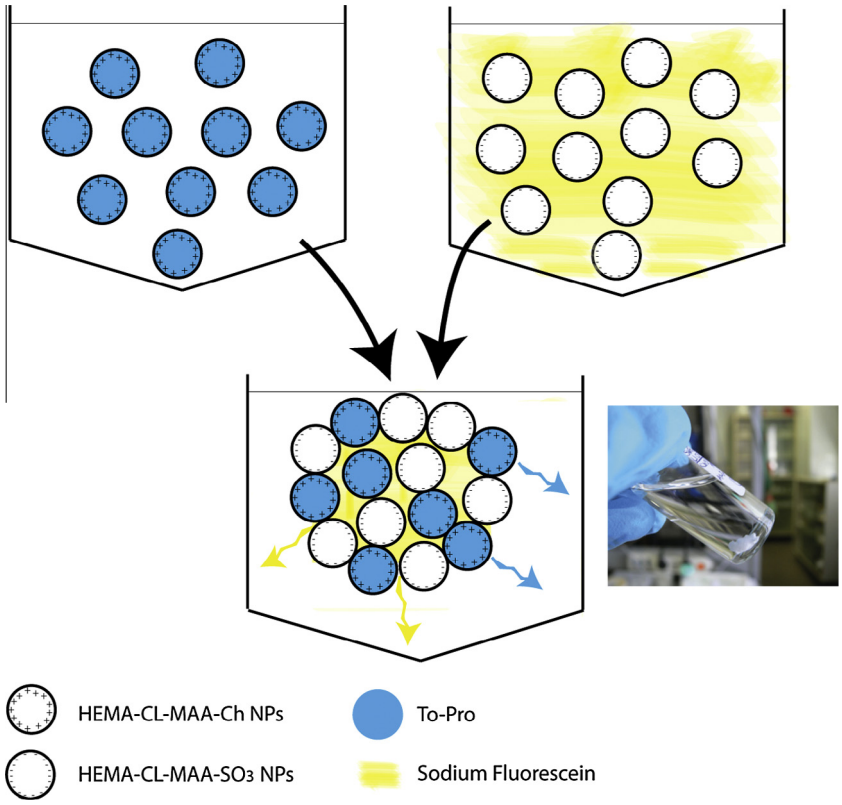

Scheme 1. Self-assembly of NPs with different superficial charges: positive NPs (HEMA-CL-MAA-Ch^{+}) and negative NPs (HEMA-CL-MAA-SO_3^-) through simply mixing at room temperature. Hydrophobic drugs (here To-Pro, blue) could be loaded within NPs, while hydrophilic (here SF, yellow) in the aqueous interstices created during the self-assembly of NPs in 3D macrostructures. (For interpretation of the references to colour in this figure legend, the reader is referred to the web version of this article.)

Hydrophilic molecules (SF) were dissolved in negatively charged NPs latex, while hydrophobic ones (To-Pro) within positively charged NPs (see Scheme 1). After NPs self-assembly, obtained dropping one latex solution into the other we are able to build a 3D macrostructure that can carry and release different water affinity solutes.

The loading percentage of SF was 62.23 ± 3.5, as detected by spectroscopy analysis of the supernatant. Fig. 5A shows a burst release of SF in the first hours due to the initial high concentration gradient, as observed also in previous works [37]. This burst could be more likely caused by: (i) molecules that were at or near the solvent-material interface and thus could rapidly escape into the supernatant solution; and (ii) molecules that found a fast path through large pores of the 3D structure, with respect of those that had to diffuse through smaller ones, thus partially suffering a constrained molecular motion. After this initial burst, release became slower and reached an almost steady state condition after about 4 days (plateau).

Moreover, it has to be noted that all the loaded SF was released: while this confirms the presence of high clearance, it also gives indirect, but very important, information about the absence of chemical stable interactions between SF and the matrix. Furthermore, SF complete release time at about 48 h, is fully compatible with medical needs on steroids like methylprednisolone [18,38,39]. For the above-mentioned considerations it can be assumed that all the loaded SF is solved within network internal medium and is free to diffuse out, driven by concentration gradients: diffusive molecules are physically entrapped inside the entangled network and are thus allowed to diffuse with a high free motion. Different is the case of To-Pro (Fig. 5B and C) that was loaded within NPs and so it needed to cross two diffusion barriers: single NP and 3D struc-ture. The loading percentage of To-Pro was 82.5 ± 2.5% as detected by spectroscopy [17]. To-Pro release, as showed from Fig. 5B, followed a biphasic pattern characterized by an initial burst release followed by a slower sustained release phase that was observed during 14 days. The percentage of To-Pro released in the first 2 h (around 25%) can be attributed either to the unloaded To-Pro, To-Pro present at the NPs surface and to the high initial concentration gradient present.

Thereon, To-Pro was slowly released through a pure Fickian diffusion phenomenon as evident from Fig. 5C, where a linear relationship between percentage released and square root time is observed. These results confirm that the release from self-assembled NPs is still mediated by Fickian diffusion [40,41]. Indeed the time-scale for degradation of the self-assembled material produced from the NPs was found to be longer respect to the characteristic time of release for both compounds and therefore degradation does not have an influence on the release, allowing pure Fickian diffusion.

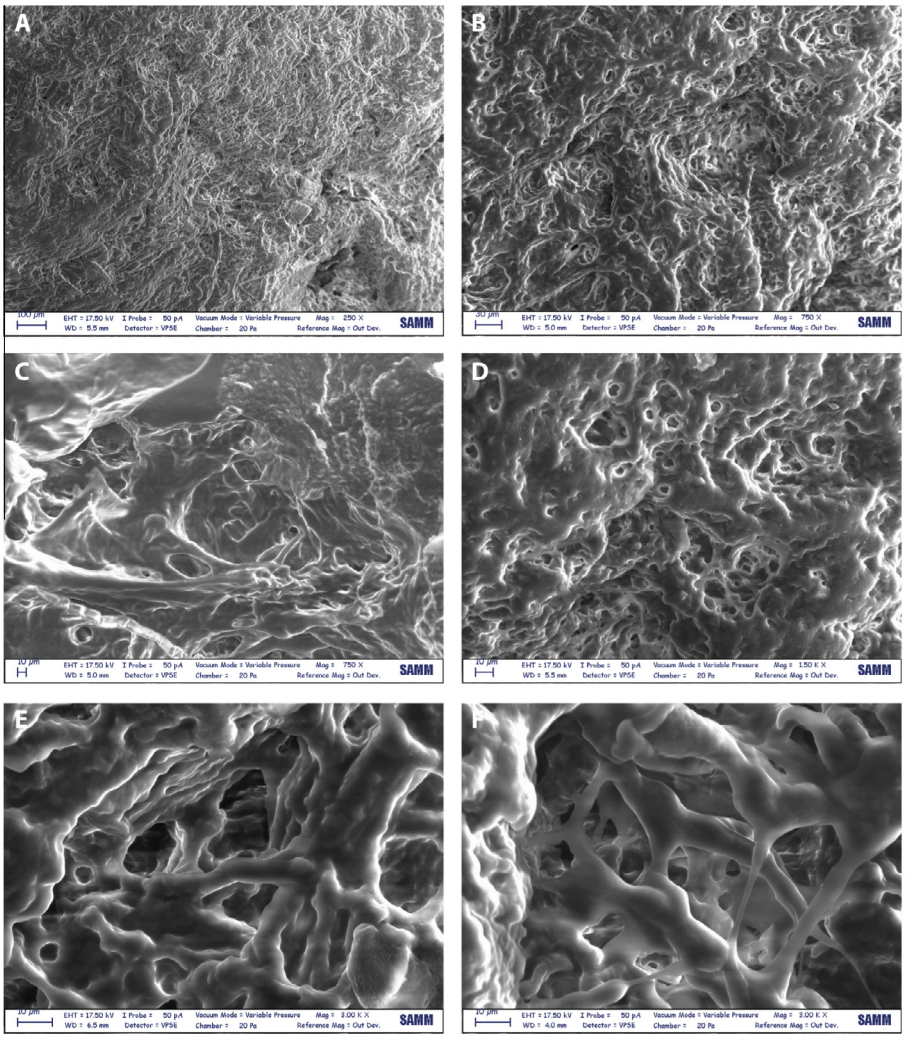

Fig. 3. SEM analysis of self-assembled network. Magnification: (A) 250×, (B and C) 750×, (D) 1500×, (E and F) 300× (scale bars: 10 μm).

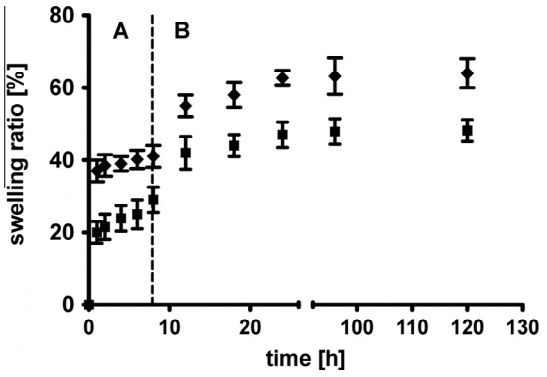

Fig. 4. Swelling kinetics of self-assembled NPs in PBS (■) and water (♦) at 37 °C.

Cytocompatibility of the macro structure was evaluated *in vitro* by culturing L929 cells for 3 days, while sharing medium with the self-assembled NPs via cell culture inserts. The corresponding NPs-forming solutions were premixed and

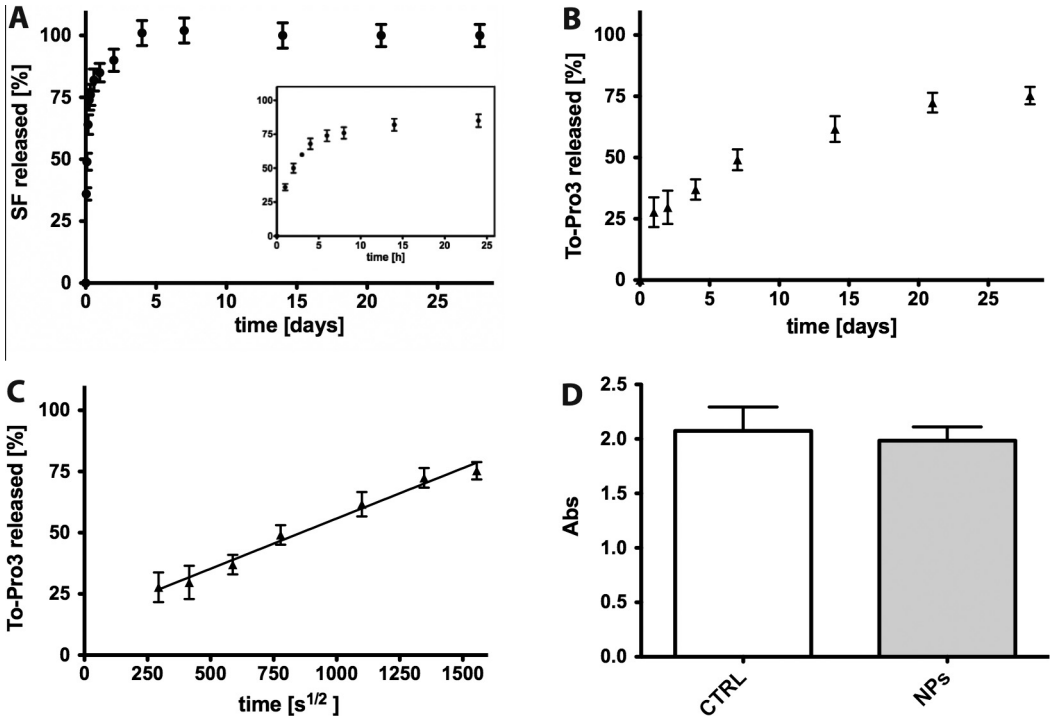

Fig. 5. (A) *In vitro* release profile of SF delivered from self-assembled NPs. The inset graph shows the detailed release profile of SF in the first 24 h. (B) *In vitro* release profile of To-Pro delivered from self-assembled NPs. (C) The slope of To-Pro release against the square root time is representative of Fickian diffusion coefficient ($p < 0.0001$). Values are calculated as percentage respect to the total mass loaded (mean value ± standard deviation are plotted). (D) L929 viability after incubation for 3 days in the presence of self-assembled NPs that were formed by combination of positive and negative NPs. The left bar corresponds to the untreated control. The columns represent the mean ± S.D.; $n = 3$.

immediately put in contact with the cell culture medium. The results shown in Fig. 5D using MTS assay clearly showed that sharing medium with NPs in all cases did not cause a decrease in cell viability.

Therefore an absence of potentially toxic components during the formation of the three-dimensional network can be confirmed.

4. Conclusions

In this study a novel self-assembled material made of single nanometric building blocks has been proposed. Oppositely charged polymer NPs were synthesized through a surfactant-free two step process that starts with the synthesis of a biodegradable macromonomer which is then polymerized in emulsion with methacrylic acid and either HEMA-Ch^+ or HEMA-SO_3^-. From NPs self-assembly, we studied the possibility to create a porous 3D macrostructure. This material presents high porosity, biocompatibility and possibility to retain aqueous solutions. In addition its ability to sustain and control the release of drugs with different nature (hydrophobic and hydrophilic) was verified. Thus, such composite material can find unique applications in cartilage or bone tissue engineering, neurological disease, spinal cord injury or tissue repair. Moreover, these novel composites can be profitably adopted in applications where different active agents should be released with independent kinetics.

Appendix A. Supplementary material

Supplementary data associated with this article can be found, in the online version.

References

[1] N.A. Peppas, Historical perspective on advanced drug delivery: how engineering design and mathematical modeling helped the field mature, Adv. Drug Deliv. Rev. 65 (1) (2013) 5–9.
[2] S. Mitragotri, J. Lahann, Materials for drug delivery: innovative solutions to address complex biological hurdles, Adv. Mater. 24 (28) (2012) 3717–3723.
[3] S. Papa, F. Rossi, R. Ferrari, A. Mariani, M. De Paola, I. Caron, et al, Selective nanovector mediated treatment of activated proinflammatory microglia/macrophages in spinal cord injury, ACS Nano 7 (11) (2013) 9881–9895.

[4] R. Shenhar, V.M. Rotello, Nanoparticles: Scaffolds and building blocks, Acc. Chem Res. 36 (7) (2003) 549–561.
[5] L.A. Sharpe, A.M. Daily, S.D. Horava, N.A. Peppas, Therapeutic applications of hydrogels in oral drug delivery, Expert Opin. Drug Deliv. 11 (6) (2014) 901–915.
[6] F. Rossi, G. Perale, S. Papa, G. Forloni, P. Veglianese, Current options for drug delivery to the spinal cord, Expert Opin. Drug Deliv. 10 (3) (2013) 385–396.
[7] J.B. Wolinsky, Y.L. Colson, M.W. Grinstaff, Local drug delivery strategies for cancer treatment: gels, nanoparticles, polymeric films, rods, and wafers, J. Control. Release 159 (1) (2012) 14–26.
[8] J. Shi, A.R. Votruba, O.C. Farokhzad, R. Langer, Nanotechnology in drug delivery and tissue engineering: from discovery to applications, Nano Lett. 10 (9) (2010) 3223–3230.
[9] N.N. Ma, C. Ma, C.Y. Li, T. Wang, Y.J. Tang, H.Y. Wang, et al, Influence of nanoparticle shape, size, and surface functionalization on cellular uptake, J. Nanosci. Nanotechnol. 13 (10) (2013) 6485–6498.
[10] R. Jeetah, A. Bhaw-Luximon, D. Jhurry, Nanopharmaceutics: phytochemical-based controlled or sustained drug-delivery systems for cancer treatment, J. Biomed. Nanotechnol. 10 (9) (2014) 1810–1840.
[11] I. Caron, S. Papa, F. Rossi, G. Forloni, P. Veglianese, Nanovector-mediated drug delivery for spinal cord injury treatment, WIREs Nanomed. Nanobiotechnol. 6 (5) (2014) 506–515.
[12] B.M. Dicheva, G.A. Koning, Targeted thermosensitive liposomes: an attractive novel approach for increased drug delivery to solid tumors, Expert Opin. Drug Deliv. 11 (1) (2014) 83–100.
[13] Y.P. Li, K. Xiao, W. Zhu, W.B. Deng, K.S. Lam, Stimuli-responsive cross-linked micelles for on-demand drug delivery against cancers, Adv. Drug Deliv. Rev. 66 (2014) 58–73.
[14] R.J. Liang, L.Y. Dong, R.H. Deng, J. Wang, K. Wang, M. Sullivan, et al, Surfactant-free biodegradable polymeric nanoparticles generated from self-organized precipitation route: cellular uptake and cytotoxicity, Eur. Polym. J. 57 (2014) 187–201.
[15] J. Nicolas, S. Mura, D. Brambilla, N. Mackiewicz, P. Couvreur, Design, functionalization strategies and biomedical applications of targeted biodegradable/biocompatible polymer-based nanocarriers for drug delivery, Chem. Soc. Rev. 42 (3) (2013) 1147–1235.
[16] M. Duran-Lobato, B. Carrillo-Conde, Y. Khairandish, N.A. Peppas, Surface-modified P(HEMA-co-MAA) nanogel carriers for oral vaccine delivery: design, characterization, and in vitro targeting evaluation, Biomacromolecules 15 (7) (2014) 2725–2734.
[17] S. Papa, R. Ferrari, M. De Paola, F. Rossi, A. Mariani, I. Caron, et al, Polymeric nanoparticle system to target activated microglia/macrophages in spinal cord injury, J. Control. Release 174 (2014) 15–26.
[18] Y.T. Kim, J.M. Caldwell, R.V. Bellamkonda, Nanoparticle-mediated local delivery of methylprednisolone after spinal cord injury, Biomaterials 30 (13) (2009) 2582–2590.
[19] F. Alexis, E. Pridgen, L.K. Molnar, O.C. Farokhzad, Factors affecting the clearance and biodistribution of polymeric nanoparticles, Mol. Pharm. 5 (4) (2008) 505–515.
[20] Y.C. Yeh, R. Tang, R. Mout, Y. Jeong, V.M. Rotello, Fabrication of multiresponsive bioactive nanocapsules through orthogonal self-assembly, Angew. Chem. Int. Ed. 53 (20) (2014) 5137–5141.
[21] J.E. Betancourt, C. Subramani, J.L. Serrano-Velez, E. Rosa-Molinar, V.M. Rotello, J.M. Rivera, Drug encapsulation within self-assembled microglobules formed by thermoresponsive supramolecules, Chem. Commun. 46 (45) (2010) 8537–8539.
[22] A. Amarjargal, L.D. Tijing, C.H. Park, I.T. Im, C.S. Kim, Controlled assembly of superparamagnetic iron oxide nanoparticles on electrospun PU nanofibrous membrane: a novel heat-generating substrate for magnetic hyperthermia application, Eur. Polym. J. 49 (12) (2013) 3796–3805.
[23] Y. Ofir, B. Samanta, V.M. Rotello, Polymer and biopolymer mediated self-assembly of gold nanoparticles, Chem. Soc. Rev. 37 (9) (2008) 1814–1823.
[24] V. Nandwana, L.A. Serrano, K.M. Solntsev, B. Ebenhoch, Q. Liu, G.Y. Tonga, et al, Engineering the nanoscale morphology of a quantum dot-fullerene assembly via complementary hydrogen bonding interactions, Langmuir 29 (24) (2013) 7534–7537.
[25] M.H. Park, C. Subramani, S. Rana, V.M. Rotello, Chemoselective nanoporous membranes via chemically directed assembly of nanoparticles and dendrimers, Adv. Mater. 24 (43) (2012) 5862–5866.
[26] S.C. Sundararaj, M.V. Thomas, R. Peyyala, T.D. Dziubla, D.A. Puleo, Design of a multiple drug delivery system directed at periodontitis, Biomaterials 34 (34) (2013) 8835–8842.
[27] Y.Z. Wang, B.C. Wang, W.L. Qiao, T.Y. Yin, A novel controlled release drug delivery system for multiple drugs based on electrospun nanofibers containing nanoparticles, J. Pharm. Sci. 99 (12) (2010) 4805–4811.
[28] R. Ferrari, Y.C. Yu, M. Morbidelli, R.A. Hutchinson, D. Moscatelli, Epsilon-caprolactone-based macromonomers suitable for biodegradable nanoparticles synthesis through free radical polymerization, Macromolecules 44 (23) (2011) 9205–9212.
[29] R. Ferrari, C. Colombo, C. Casali, M. Lupi, P. Ubezio, F. Falcetta, et al, Synthesis of surfactant free PCL–PEG brushed nanoparticles with tunable degradation kinetics, Int. J. Pharm. 453 (2) (2013) 551–559.
[30] M. Santoro, P. Marchetti, F. Rossi, G. Perale, F. Castiglione, A. Mele, et al, Smart approach to evaluate drug diffusivity in injectable agar–carbomer hydrogels for drug delivery, J. Phys. Chem. B 115 (11) (2011) 2503–2510.
[31] R. Ferrari, Y. Yu, M. Lattuada, G. Storti, M. Morbidelli, D. Moscatelli, Controlled PEGylation of PLA-based nanoparticles, Macromol. Chem. Phys. 213 (19) (2012) 2012–2018.
[32] D.A. Ossipov, S. Piskounova, O.P. Varghese, J. Hilborn, Functionalization of hyaluronic acid with chemoselective groups via a disulfide-based protection strategy for in situ formation of mechanically stable hydrogels, Biomacromolecules 11 (9) (2010) 2247–2254.
[33] J. Zhu, C. Tang, K. Kottke-Marchant, R.E. Marchant, Design and synthesis of biomimetic hydrogel scaffolds with controlled organization of cyclic RGD peptides, Bioconjugate Chem. 20 (2) (2009) 333–339.
[34] M. Bongio, M.R. Nejadnik, Z.T. Birgani, P. Habibovic, L.A. Kinard, F.K. Kasper, et al, In vitro and in vivo enzyme-mediated biomineralization of oligo(poly(ethylene glycol) fumarate hydrogels, Macromol. Biosci. 13 (6) (2013) 777–788.
[35] J. Magalhaes, R.A. Sousa, J.F. Mano, R.L. Reis, F.J. Blanco, J. San Roman, Synthesis and characterization of sensitive hydrogels based on semi-interpenetrated networks of poly[2-ethyl-(2-pyrrolidone) methacrylate] and hyaluronic acid, J. Biomed. Mater. Res. Pt A 101 (1) (2013) 157–166.
[36] Q. Xing, K. Yates, C. Vogt, Z. Qian, M.C. Frost, F. Zhao, Increasing mechanical strength of gelatin hydrogels by divalent metal ion removal, Sci. Rep. 4 (2014) 4706.
[37] G. Perale, F. Rossi, M. Santoro, M. Peviani, S. Papa, D. Llupi, et al, Multiple drug delivery hydrogel system for spinal cord injury repair strategies, J. Control. Release 159 (2) (2012) 271–280.
[38] K. Cao, L. Huang, J.W. Liu, H. An, Y. Shu, Z.M. Han, Inhibitory effects of high-dose methylprednisolone on bacterial translocation from gut and endotoxin release following acute spinal cord injury-induced paraplegia in rats, Neur. Regen. Res. 5 (6) (2010) 456–460.
[39] M.B. Bracken, M.J. Shepard, W.F. Collins, T.R. Holford, W. Young, J. Piepmeier, et al, A randomized, controlled trial of methylprednisolone or naloxone in the treatment of acute spinal-cord injury, New England J. Med. 323 (17) (1990). 1209-1209.
[40] K. Vulic, M.S. Shoichet, Tunable growth factor delivery from injectable hydrogels for tissue engineering, J. Am. Chem. Soc. 134 (2) (2012) 882–885.
[41] P.L. Rither, N.A. Peppas, A simple equation for description of solute release I. Fickian and non-Fickian release from non-swellable devices in the forms of slabs, spheres, cylinders or discs, J. Control. Release 5 (1) (1987) 23–36.